SSRG International Journal of Mechanical Engineering
ISSN: 2348-8360/ https://doi.org/10.14445/23488360/IJME-V12I4P103

Volume 12 Issue 4, 20-36, April 2025

Original Article

Effects of the Nano-Fe_3O_4 Embedded Beeswax PCM's Thermal Storage Characteristics on the Performance of the 2% Hybrid Nano Coating Solar Water Heater by the Approach of Box-Behnken Design

N.V. Narasimha Rao[1], N. Alagappan[1], CH V K N S N Moorthy[2], Markndeyulu Vuggirala[3]

[1]*Department of Mechanical Engineering, Annamalai University, Chidambaram, Tamil Nadu, India.*
[2]*Department of Mechanical Engineering, Vasavi College of Engineering, Ibrahimbagh, Hyderabad, Telangana, India.*
[2]*Department of Mechanical Engineering, St. Ann's College of Engineering and Technology, Chirala, Andhra Pradesh, India*.

[2]*Corresponding Author : krishna.turbo@gmail.com*

Received: 03 February 2025 Revised: 04 March 2025 Accepted: 05 April 2025 Published: 30 April 2025

Abstract *- Solar energy is a plentiful and dependable source for power generation and heating. The present study investigates the enhancement of heat storage qualities by the unique class of Nano-Embedded Bees Wax Phase Change Materials (NEBPCMs). Fourier Transform Infrared Spectroscopy (FT-IR) Differential Scanning Calorimetry (DSC) was used to evaluate the synthetic NEBPCMs experimentally. A typical solar water heating system features a flat plate collector unit incorporating Nano Bees Wax phase change material (NEBPCM) combined with varying concentrations of Fe_3O_4 (0.01%, 0.015%, and 0.02%). The absorber plate surface is coated with a Nano-hybrid coating consisting of Black Paint, Al_2O_3, and additional Fe_3O_4 at 2% concentration. Pure water is frequently used in these Solar Water Heaters (SWH), with performance evaluations conducted using NEBPCM (Bees Wax + Fe_3O_4). The system's efficiency is assessed across different flow rates (60, 90, and 120 kg/hr) and tilt angles (15, 30, and 45 degrees). The purpose of this study is to determine whether it is feasible to use PCMs to store solar energy for water heating at night in order to ensure a continuous supply of hot water, with maximum efficiency achieved by using NEBPCM in solar water heater 54.95% at a flow rate of 120 Kg/hr, at an angle of 45 Degrees and Concentration 0.015%.*

Keywords *- SWH, BBD, Hybrid surface coating, NEBPCM, Collector performance, Optimum flow rate, Optimum angle, Optimum concentrations, Heat transfer fluid.*

1. Introduction

Solar energy is abundant, free and environmentally friendly as a Renewable Energy Source (RES). Solar collectors can be used to transform Solar Energy (SE) into Thermal Energy (TE). Energy demands are rising significantly each year as a result of the world's population expansion, industrialization, and rapid urbanization [1]. However, according to the World Health Organization (WHO), air pollution alone claims the lives of almost seven million people worldwide each year. This terrible phenomenon is caused by the burning of fossil fuels to meet energy demands, mostly for transportation, heating, and power generation [2]. Additionally, using fossil fuels results in the production of greenhouse gases, which gradually raise the global temperature [3-5]. The nation's daunting task is to meet the growing demand for energy without causing more harm to our planet. In light of these considerations, the nations are continuously succeeding in structuring their energy policies to promote the production of energy from Renewable Sources (RS) [6]. Reports indicate that Thermal Energy (TE) is the most widely used and vital form of energy across commercial, industrial, and residential sectors. Globally, approximately 50% of all energy produced is dedicated to heating applications, such as space heating, industrial processes, drying, and domestic hot water needs. Furthermore, forty-six of thermal energy is specifically consumed for water heating in various industries and daily activities.

This includes preheating boiler water in power plants, as well as applications in cooking, bathing, cleaning, and industrial processes such as food processing, paper pulp production, textile manufacturing, leather treatment, and rice milling [7]. The data reveals that a substantial portion of globally produced energy primarily derived from fossil fuels is consumed for heating applications. Shifting to direct heat sources, particularly those powered by renewables, could drastically reduce grid electricity demand and minimize biosphere emissions. A promising solution is Solar Thermal Conversion (STC) coupled with an efficient Solar Collector (SC). This system harnesses freely available and abundant

solar radiation to generate the required Heat Energy (HE), offering a sustainable alternative to conventional heating methods [8]. WGSWHs are gaining a lot of attention these days due to their low maintenance requirements, superior efficiency, easy construction, and affordable price. Specifically, because of their economics, gravity-driven flow-based SWHs are widely valued by both residential and commercial sectors [9, 10]. Nevertheless, these water heaters also have intrinsic drawbacks: they are unable to balance supply and demand because of erratic climate conditions, and they suffer from losses and LES (Low Energy Storage) density [11, 12].

Potential Phase Change Materials (PCMs) were recommended as a means of efficiently enhancing the high calorie and heat direction of SWHs [13, 14] and survey article [15, 16]. Compared, under constant flow rate conditions, the effectiveness of conventional ET-SWHs with a residential SWH that is PCM linked. He integrated barium hydroxide, which he used as PCM, inside the evacuated tubes. [17]. Developed a Solar Water Heater (SWH) using an (HPC) Heat Pipe Collector and examined how the performance of the SC (solar collector) was affected by using paraffin as Phase Change Materials (PCM). They admitted that the phase change materials had reduced the variability in connoisseur effectiveness related to changes in Solar Intensity (SI) and that it had also quickly raised the temperature of the outflow water [18].

The recent reviews. [19, 20] Distinct thermo-physical characteristics of paraffin-based PCMs, including their adjustability for diverse applications, ensuring material compatibility, enabling efficient energy storage, heat endurance, reduced supercoiling and affordability, define them. Nevertheless, due to its poor thermal conductivity, paraffin is strongly discouraged. [21-23]. Additionally, the issue was tackled by including copper flats [24], using media with pores [25], and dissolving magnetic nanomaterials [26].

The migration of nanocrystals within the starting fluid has the potential to be the most effective way to increase fluids' heat conductivity more favourably among the many suggested approaches [27-29]. Revealed that using graphene nano-platelets increased the paraffin's heat conductivity by eleven hundred percentage [30].

Recognized that the addition of tiny particles of copper II oxide to paraffin increased its ability to conduct heat. However, their study did not mention the proportion of enhancement. The impact of three different kinds of nanoparticles, copper II oxide, titanium IV oxide, and Al_2O_3 (Aluminium oxide), on the TS (Thermal storage) characteristics of paraffin was covered in different research [31].

This paper's unique goal is to examine the real-time performance of flat plate collector SWHs under the impact of the aforementioned Fe_3O_4 ultrafine grains incorporated in beeswax in a two percent hybrid nanocoating on absorber plate situation, as well as to investigate the heating features of beeswax when incorporated various percentages of Fe_3O_4 zero-dimensional, that's never to be described in the scientific community.

2. Research Gap

Most existing studies focus on paraffin-based or salt-hydrate Phase Change Materials (PCMs), with the limited investigation into beeswax-based PCMs enhanced with magnetic nanoparticles such as Fe_3O_4. While hybrid nanocoatings (e.g., TiO_2, SiO_2, Fe_3O_4) for solar water heaters have been studied for thermal efficiency, the optimal nanoparticle concentration remains unclear. Additionally, there is a lack of comparative studies between Fe_3O_4-beeswax PCMs and other nanomaterial-enhanced PCMs (Al_2O_3, CuO, graphene). Although the Box-Behnken Design (BBD) is employed for optimization, existing research often neglects the interactions among key parameters such as Fe_3O_4 mass fraction, beeswax-to-PCM ratio, and coating thickness that influence thermal performance.

3. Novelty of the Work

Previous research has predominantly explored conventional Phase Change Materials (PCMs) such as paraffin, salt hydrates, and fatty acids for thermal energy storage. Beeswax, a bio-based PCM, remains understudied, particularly when enhanced with Fe_3O_4 nanoparticles for improved thermal conductivity and latent heat storage in solar water heating systems. This study introduces an innovative approach by combining Fe_3O_4 nanoparticles with beeswax-based PCM, presenting a sustainable and high-performance alternative for thermal energy storage. Existing studies on nanocoatings for solar water heaters have largely focused on single nanoparticles like TiO_2 or SiO_2. In contrast, this work investigates a novel 2% hybrid nanocoating (Al_2O_3 + Fe_3O_4) designed to synergistically enhance solar absorption, heat retention, and overall system efficiency. Furthermore, the research provides new insights into the influence of nanocoating on heat transfer dynamics, PCM charging/discharging rates, and long-term system durability, addressing critical gaps in solar thermal energy research.

4. Phase Change Materials

The selection of Phase transition materials is based on their economics, kinetics, chemistry, and thermo-physical characteristics. Solid-Solid (S-S) phase-changing materials, Solid-liquid (S-L) phase-changing materials, and Solid-Gas (S-G) phase-changing materials are the three types of Phase transition materials. Solid-Liquid (S-L) PCMs are used more often than any other of the three groups.

Table 1. Existing literature review on PCM

Author name	Collector type	PCM Description	Parameter studied	Major findings	References
Fazilati (2013)	The amount of energy stored per unit volume or mass of a material.	Thermal energy during phase transitions	effectiveness of container consistency	This demonstrates PCM's potential to optimize thermal energy storage systems by maximizing energy retention and thermodynamic efficiency.	32
Serali (2014)	PCM slurry-based collector	Phase transition material slush	identified the optimal melting point to maximize thermal energy utilization while ensuring compatibility with operational conditions	Analysis of system performance reveals a statistically significant increase in instantaneous efficiency, with measured improvements falling within the 5-10% range under standard operating conditions.	33
Yang (2014)	PCM in container	Synthesized trilogy categories of spherical encapsulated Phase transition material	PCM liquefy temperature	The hybrid PCM system demonstrates higher overall thermal efficiency but exhibits bottommost concentrated energy effectiveness when collated to solitary-phase transition material configurations.	34
Nandy Putra1 (2016)	Thermal Storage	beeswax/CuO nano-PCM	Thermal capacity of beeswax/CuO nano-PCM	study the thermal properties of nano-PCM for low-temperature application	35
P. Manoj Kumar (2019)	Evacuated tube	Paraffin wax as PCM and incorporate nanoadditives of paraffin wax	Temperatures, efficiency and thermal conductivity	The NCPCM configuration demonstrated the highest performance gains, achieving a 27.3% increase in energy efficiency and 25.5% in exergy efficiency compared to the baseline.ss	36

5. Materials, Preparation and Characterization of PCM and Nano embedded Bees wax PCM (NEBPCM)

5.1. Materials

5.1.1. Bees Wax Phase Change Material

Bees use wax to construct combs in which they store their pollen, honey, and young. Worker bees release beeswax in the form of wax scales from their wax glands, which are located on the underside of the abdomen in the front portion of the sterna from segments IV to VII. Between ten and fifteen parts of honey are thought to be required by bees to generate one component of wax. Sometimes, wax is also applied to the matured honey. Beeswax's chemical formula is $C_{15}H_{31}COOC_30H_{61}$. Figure 1 shows the Solid beeswax Phase change material.

Fig. 1 Solid bees wax PCM

5.1.2. Nanomaterials

Nanomaterials are generally defined as materials having a structure of 100 nm or less. These materials might take the form of particles, tubes, rods, or threads. Fe_3O_4 is a nanoparticle and structure of iron II, III oxide. Fe_3O_4, an iron ore, is also known as magnetite. They are among the substances that are found in nature the most frequently. Because of the way the compound looks, iron oxide is often referred to as black iron oxide. Iron can create a variety of oxides, including Fe_3O_4. The most popular application for iron oxide (Fe_3O_4) is as a black pigment. It is deep black in colour and glows metallically. Figure 2 shows the Fe_3O_4 nanoparticle and structure.

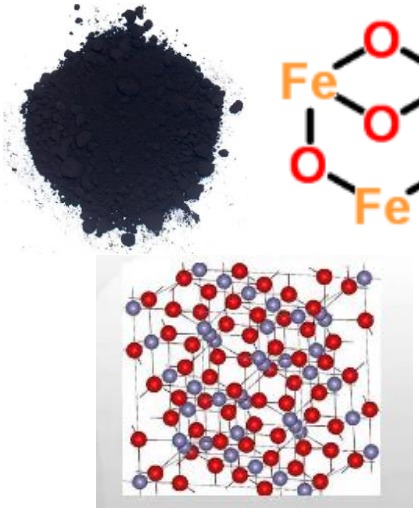

Fig. 2 Fe_3O_4 nanoparticle and structure of Fe_3O_4

Table 2. Properties of the Fe_3O_4 nanoparticle

Property	Fe3O4
Purity	98.45%
Size	18-28 nm
Density	5170 Kg/m^3
Melting Point	1,597 °C (2,907 °F)
Specific heat	670 J/kg k
Thermal conductivity	1631 W/m k

5.2. Preparation and Characterization Beeswax PCM

Raw beeswax, collected from honeycomb cappings, is first melted in hot water maintained at 60–70°C to separate the wax from impurities. Once purified, the liquid wax is carefully poured into moulds and left to cool at room temperature until it solidifies into usable blocks or forms.

A FESEM was used to examine the samples after their surfaces had been coated with gold to make them conductive. Because scanning electrons have a high energy, low-resolution scanning was employed to take the photos to save the beeswax from melting. The photographs of the samples show that the beeswax structure is typically built straight up Figure 3.

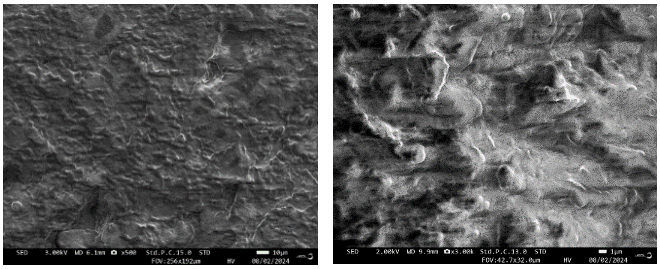

Fig. 3 Bees wax field emission scanning electron microscope for 10 and 100 µm

Table 3. Thermal & physical property comparison with traditional PCM

Property	Beeswax PCM	Paraffin Wax PCM
Latent Heat (J/g)	170–230 J/g	150–220 J/g
Thermal Conductivity (W/mK)	0.24 W/mK	0.21-0.24 W/mK
Melting Point (°C)	61–65^{0}C	45–65^{0}C
Supercooling Effect	Minimal	No effect
Phase Separation	No	No
Thermal Stability	High	Moderate
Environmental Impact	Biodegradable	Petroleum-based

5.3. Preparation and Characterization NEBPCM

The preparation of Nano-Embedded Beeswax PCM (NEBPCM) involves the dispersion of Fe_3O_4 nanoparticles into beeswax. Fe3O4 nanoparticle dispersion in 10 kgs of Bees wax phase change material using weight volume analysis (0.01%, 0.015%, 0.02%). Melt beeswax in a hot plate or oil bath at 70-80°C, ensuring uniform heating. Maintain the gentle stirring to prevent thermal degradation.

Fe_3O_4 nanoparticles are gradually added to the molten beeswax under continuous mechanical stirring (1000–1500 rpm for 30–60 minutes) to ensure homogeneous dispersion. The mixture is cooled either at room temperature or via a controlled cooling rate (10°C/min) to minimize nanoparticle sedimentation.

The solidified Nano-Embedded Beeswax PCM (NEBPCM) has been obtained and is ready for integration into solar water heating systems. Figure 4 shows the making of NEBPCM using a two-step process, and Figure 5 shows the steps to prepare nano-embedded Bees wax PCM.

Fig. 4 Making NEBPCM using a two-step process

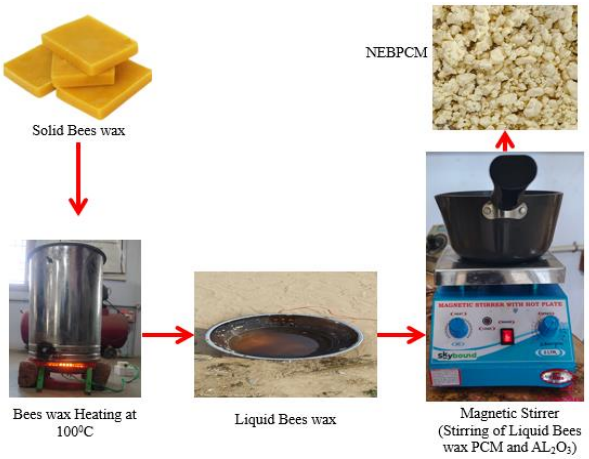

Fig. 5 Steps prepare nano embedded beeswax PCM

The improvement of the thermo-physical characteristics of the produced materials (beeswax and NEBPCM) in small amounts was seen using a range of characterization tools. Some of the tests carried out at CSIR-Central Electrochemical Research Institute (CECRI) at Karaikudi include Fourier Transform Infrared Spectroscopy (FT-IR) Differential Scanning Calorimetry (DSC).

6. Experimental Setup

The experimental setup, shown in Figure 6, consists of a 100-liter water tank mounted on a table and connected to a pump and rotameter. The system includes a frame adjustable to angles of 15°, 30°, and 45°. The rotameter regulates the water flow rate, which is directed through a pipe to a flat plate collector at three specific flow rates: 60, 90, and 120 kg/hr. The setup uses copper tubes with a circular cross-section and an outer diameter of 10 mm. Each tube is 2 meters long and fitted with 1 mm thick, corrugated black-painted fins that are 75 mm wide. The top and bottom headers are also made of copper tubing with an outer diameter of 25 mm.

As water flows through the copper tubes, it is heated by the absorber plate. Temperature readings are recorded using twelve K-type thermocouples positioned at various points: for water inlet and outlet, nano-embedded beeswax Phase Change Material (PCM), the glass top surface, the absorber plate, the space between the glass and absorber plate, ambient air, and five locations along the copper tubes. Measurements are taken hourly.

Figure 7 shows the experimental setup positioned outdoors, aligned from north to south, to collect data. Figure 8 and 9 illustrate the Nano-Embedded Beeswax PCM (NEBPCM), a phase change material mixed with Fe_3O_4 nanoparticles in concentrations of 0.01%, 0.015%, and 0.02%. This NEBPCM absorbs heat from the copper tubes and absorber plate during the day, storing it for gradual release at night.

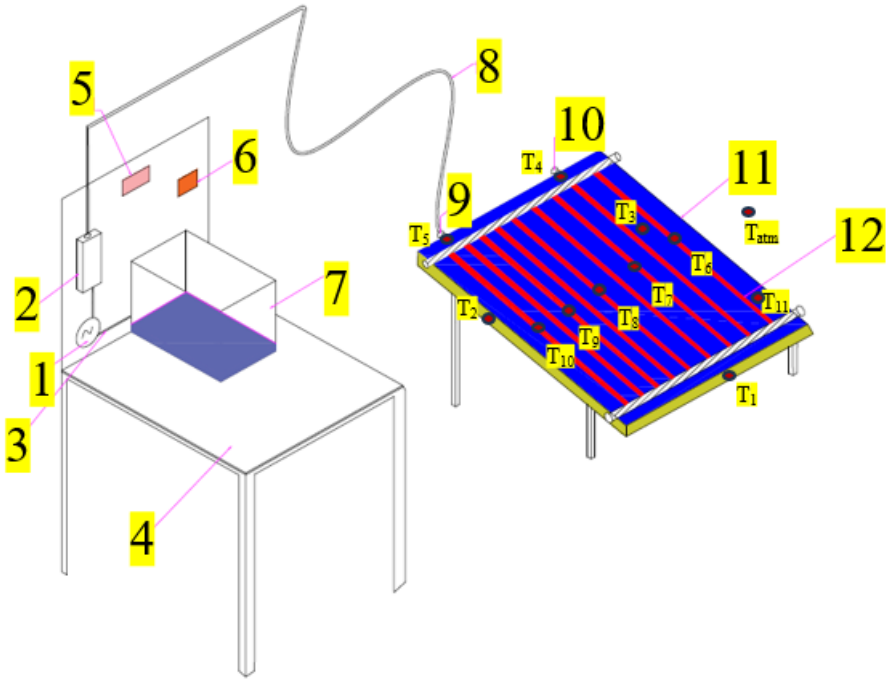

1. Pump 2. Rotameter 3. Tank to Pump Water Pipeline 4. Table 5. Temperature Knob 6. Temperature Indicator 7. Water tank 8. Rotameter to flat plate collector water pipeline 9. Flat plate Collector inlet10. Flat plate collector outlet 11. Flat plate collector 12. Copper tubes

Fig. 6 Experimental setup

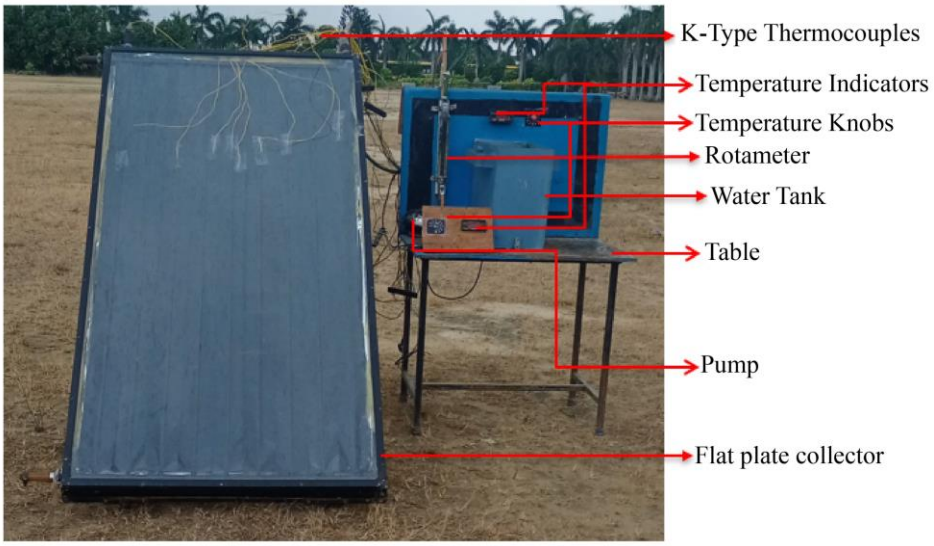

Fig. 7 Experimental setup with names

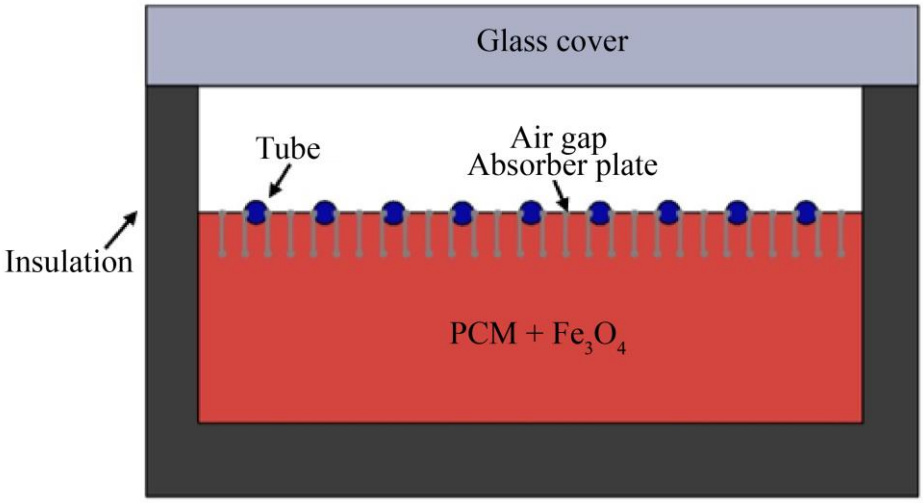

Fig. 8 Flat plate collector with NEBPCM

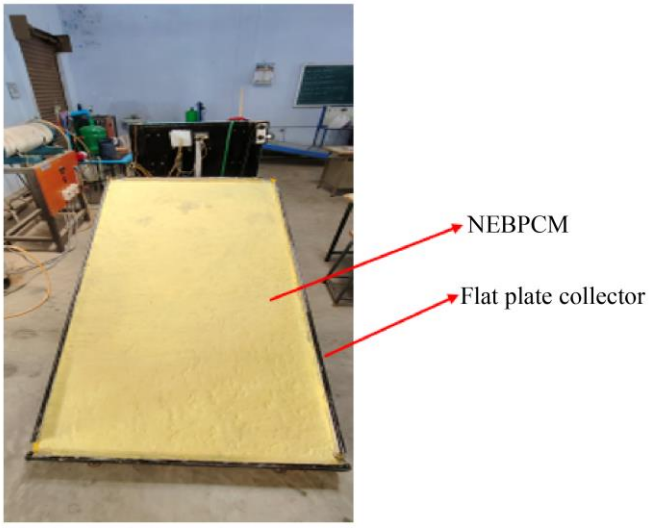

Fig. 9 NEBPCM for the bottom of the absorber plate

6.1. Box-Behnken Design

The Box-Behnken design is effective for the response surface method because it enables the following tasks

- Parameter estimation for the quadratic model
- Making designs in a sequential manner
- By using blocks
- Determining when the model is not applicable to the data.

6.1.1. Measurable and Control Variables their Levels

Table 4. Measurable and control variables

Measurable and control variables	Level (-1)	Level (0)	Level (1)
Flow rate (kg/hr)	60	90	120
Angle of Inclination (degrees)	15	30	45
Concentration (%)	0.01	0.015	0.02

6.1.2. Design of Matrix

The Design of Experts (DOE) is a useful tool for setting up trials and quickly analyzing the data they collect. The first step in an experiment is to choose the variables that will be fed in and the reaction that will be measured. As shown in Table 3 below, BBD ran 17 simulations on a copper-absorbing plate with a Hybrid nanocoating and NEBPCM. The runs were grouped by three factors.

Table 5. Design of matrix

		Factor 1	Factor 2	Factor 3	Response 1	Response 2
Std	**Run**	**A: FLOW RATE**	**B: ANGLE**	**C: CONCENTRATION**	**EFFICIENCY**	**Qc**
		Kg/hr	**Degrees**	**%**	**%**	**Kw**
4	1	120	45	0.015	54.95	3.49615
14	2	90	30	0.015	39.06	3.044
12	3	90	45	0.02	47.84	3.044
9	4	90	15	0.01	32.55	2.826
3	5	60	45	0.015	37.59	2.391
8	6	120	30	0.02	46.73	3.641
17	7	90	30	0.015	39.06	3.044
15	8	90	30	0.015	39.06	3.044
13	9	90	30	0.015	39.06	3.044
16	10	90	30	0.015	39.06	3.044
5	11	60	30	0.01	29.76	2.319
11	12	90	15	0.02	35.05	3.044
6	13	120	30	0.01	52.33	4.078
1	14	60	15	0.015	21.7	1.884
10	15	90	45	0.01	46.13	2.935
2	16	120	15	0.015	38.58	3.351
7	17	60	30	0.02	26.97	2.101

6.2. NEBPCMs' Thermal Storage Characteristics

6.2.1. FT-IR of NEBPCM

The FT-IR spectrum of Fe_3O_4-NEBPCM is shown in Figure 10, along with its distinctive functional vibrations and intrinsic peaks at different wavenumbers. It was distinguished by two strong peaks located at 2851.63 cm^{-1} and 2921.01 cm^{-1}, respectively, which showed a firm asymmetric widening vibration of carbon-hydrogen molecules and a mild symmetrical widening vibration. Similarly, strident spots have been identified at 723.84 cm^{-1} and 1174.11 cm^{-1}, indicating intermediate scissor vibration of Iron II III Oxide molecules and moderate swaying skeleton vibration of iron-iron molecules, respectively. Without alteration, the previously specified wavenumbers have been consistently detected in 0.2% of the sample. However, as shown in Figure, a distinct tiny dale point was found in the samples made of Fe_3O_4 nanoparticles at the wavenumber of 453.62 cm^{-1}.

6.2.2. DSC of NEBPCM

In order to melt the NEBPCM (Beeswax PCM+0.2% Fe_3O_4) for the thermal cycling testing, the thermostatic oven's temperature was maintained at approximately 100^0C. For air cooling Figure 11, the NEBPCM's melting temperature and latent heat of fusion were 41.92°C and 97.56 kJ kg^{-1}, while for N2 cooling Figure 12, they were 44.33°C and 73.73 kJ kg^{-1}, respectively. The time taken by the NEBPCM was approximately 35 and 50 min for melting and cooling.

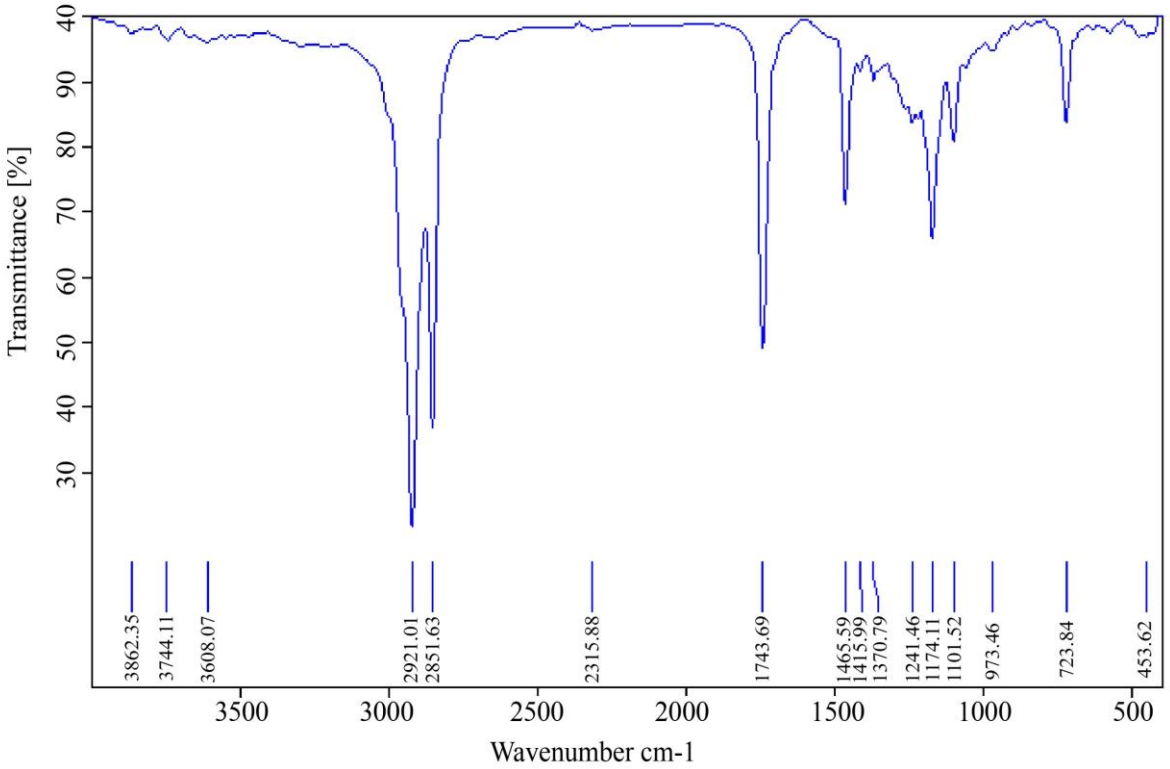

Fig. 10 0.2% NEBPCM (Bees wax + Fe_3O_4) Fourier Transform Infrared Spectrometer (FT-IR)

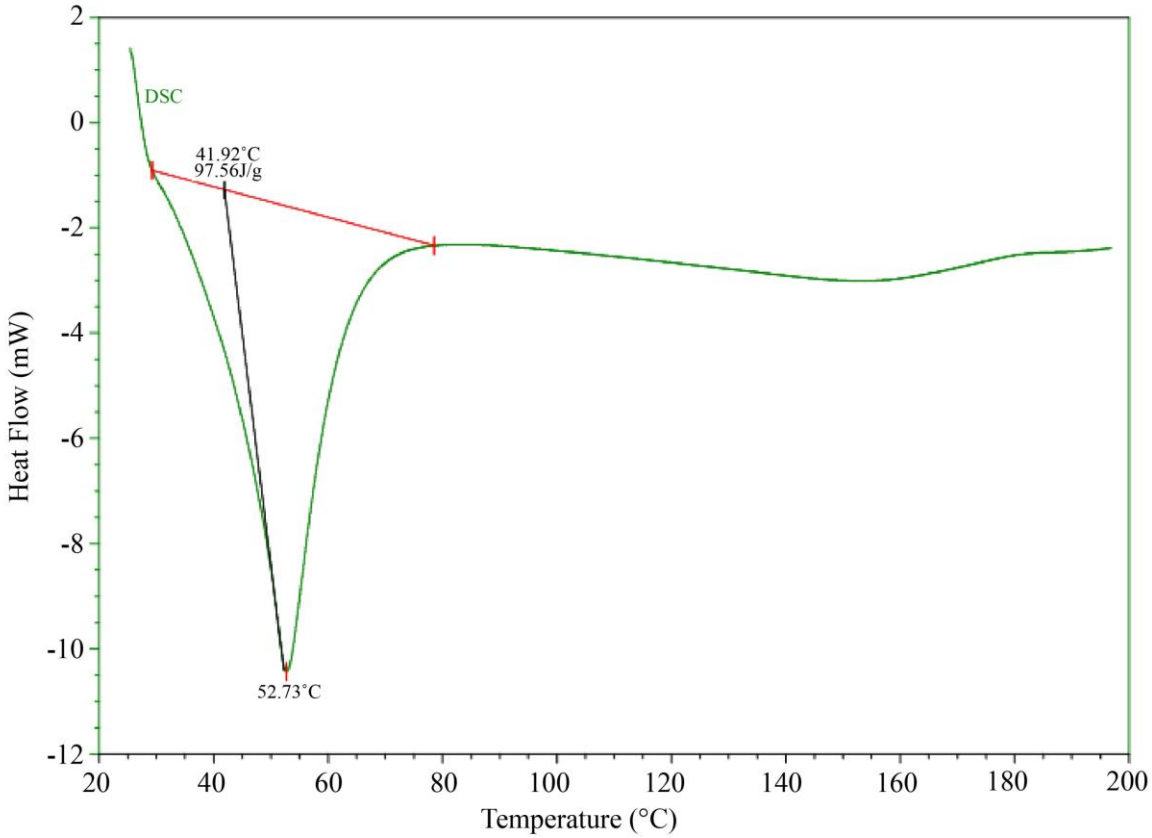

Fig. 11 0.2% of NEBPCM (Bees wax + Fe_3O_4) Differential Scanning Calorimetry (DSC) air cooling

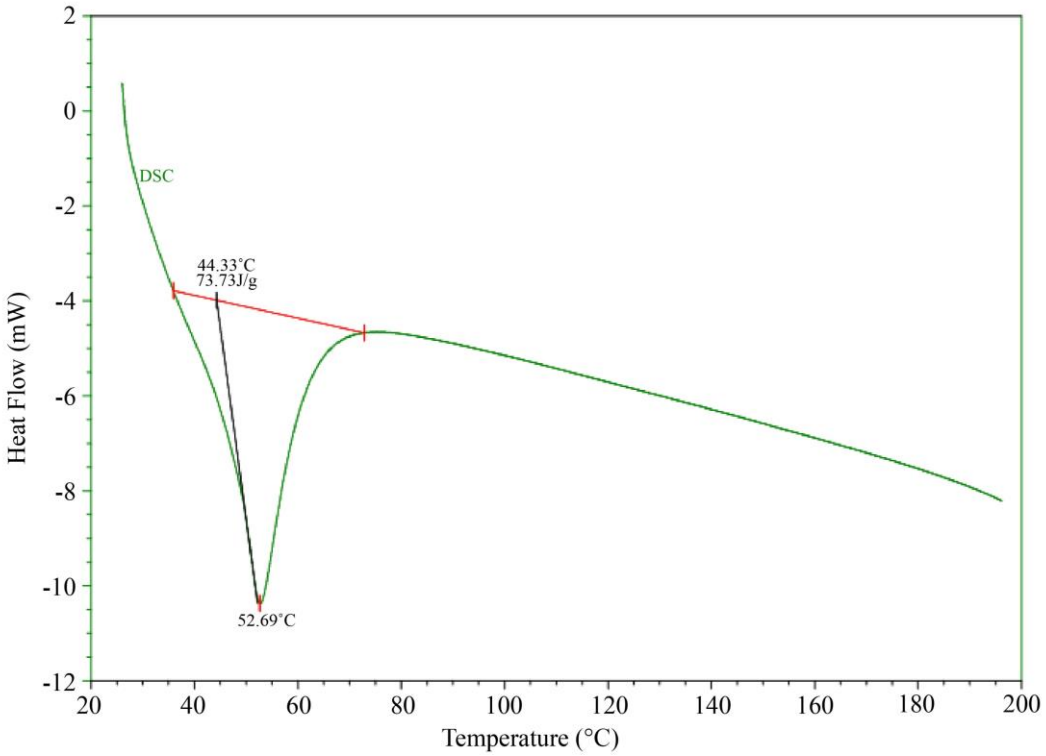

Fig. 12 0.2% of NEBPCM (Bees wax + Fe_3O_4) Differential scanning calorimetry (DSC) nitrogen gas cooling

6.3. Formulas

The percentage of thermal efficiency (η%) of the Flat plate collector is determined by

1. Energy that can be used or heat gained by the operating fluid:

$$Q_c = m_c C_{pc} (\Delta T) \text{ Watts}$$

2. Heat hold by the collector:

$$Q_a = I \times A \text{ watts}$$

3. Efficiency of the unit: (η%) = heat gained by the operating fluid / Heat hold by the collector ×100

4. Estimation of Nanoparticle Volume Concentration

$$\% \text{ volume concentration} = \frac{\frac{W_p}{\rho_p}}{\frac{Wp}{\rho_p} + \frac{W_f}{\rho_f}}$$

6.4. Uncertainty Analysis

To determine derived quantities in thermodynamic modelling, we employ experimental uncertainty analysis following established metrological principles. In this work, the system efficiencies have been the function of the Mass flow of cold fluid (m_e), the energy that can be used or heat gained by the operating fluid (Q_c) and Heat held by the Collector's Heat (Q_a).

The relative uncertainty for η % is evaluated by Equation (1),

$$\eta\ \% = f(m_e, Q_c, Q_a)$$

$$e = \frac{\partial \eta}{\eta} = \sum_{i=1}^{N} \left(\frac{1}{\eta} \, X \frac{\partial R}{\partial xi} \, X \, \partial xi \right)$$

$$= \left(\frac{\partial m}{m} \right) + \left(\frac{\partial Qc}{Qc} \right) + \left(\frac{\partial Qa}{Qa} \right) \quad (1)$$

The largest uncertainty associated with the results of η% values was approximately 1.42% when η was calculated for the whole experimental range.

7. Results and Discussions

7.1. Effect of Thermal Efficiency (η %) on Various Input Parameters of NEBPCM (Bees wax + Fe_3O_4) and 2% Hybrid Nanocoating with Working Fluid as Water

Table 6 displays the findings of the ANOVA that was performed on the data collected for the experiment. The gotten F-value of 28.28 implies the model is substantial. There is only a 0.01% chance that an F-value this large could occur due to noise. "Prob > F" less than 0.0500 shows that the model terms are important. The model's goodness of fit can be explained by the R^2, which in this occurrence is 0.9732. This suggests that less than 5% of the variances are not explained by the model and that ninety percentage of the results from the

experiment were consistent with the data anticipated adjacent to the approach. When compared to the predicted R^2 (0.5718), the modified R^2 value (0.9388) is reasonable. Adequate precision is used to measure to be 20.4960, which amply demonstrates that the model is sufficient. Equation (2) contains the final equation produced by DOE.

Table 6. ANOVA table for efficiency (Response1)

Response 1 **Efficiency (η %)** **ANOVA for Response Surface Quadratic Model** **Analysis of variance table [Partial sum of squares – Type III]**						
Source	**Sum of Squares**	**df**	**Mean Square**	**F-value**	**p-value Prob > F**	
Model	1176.88	9	130.76	28.28	0.0001	significant
A-FLOW RATE	732.87	1	732.87	158.52	< 0.0001	
B-ANGLE	429.68	1	429.68	92.94	< 0.0001	
C-CONCENTRATION	2.18	1	2.18	0.4724	0.5140	
AB	0.0576	1	0.0576	0.0125	0.9143	
AC	1.97	1	1.97	0.4270	0.5343	
BC	0.1560	1	0.1560	0.0337	0.8595	
A^2	5.57	1	5.57	1.20	0.3087	
B^2	0.3664	1	0.3664	0.0793	0.7864	
C^2	4.53	1	4.53	0.9803	0.3551	
Residual	32.36	7	4.62			
Lack of Fit	32.36	3	10.79			
Pure Error	0.0000	4	0.0000			
Cor Total Std.Dev	1209.24 2.15	16	R-Squared	0.9732		
Mean	39.15		Adjusted R^2	0.9388		
C.V. %	5.49		Predicted R^2	0.5718		
PRESS	517.80		Adeq Precision	20.4960		

Final equation in terms of coded factors: Efficiency = 39.06 + 9.57125 * A + 7.32875 * B + -0.5225 * C + 0.12 * AB + -0.7025 * AC + -0.1975 * BC + -1.15 * A^2 + 0.295 * B^2+ 1.0375 * C^2 (2)

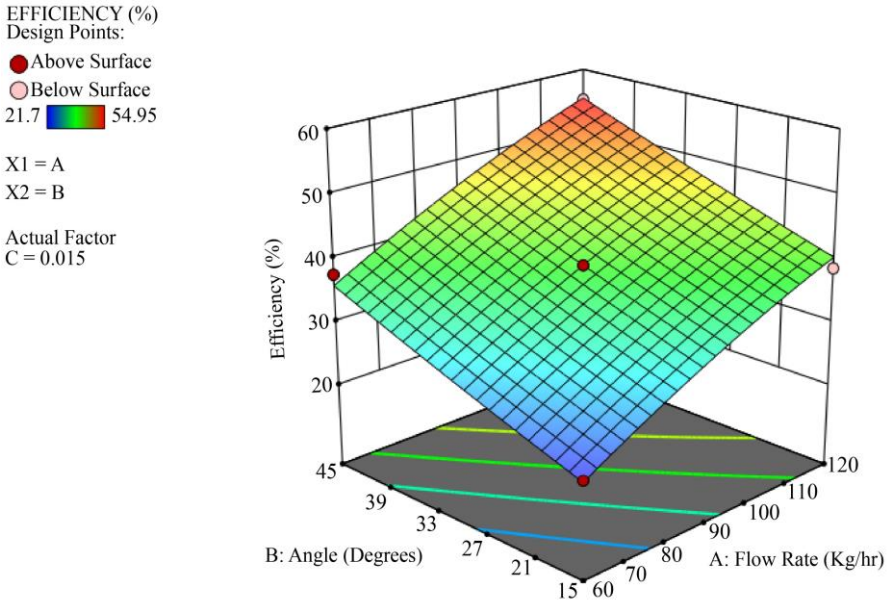

Fig. 13 Efficiency with respect to angle and flow rate

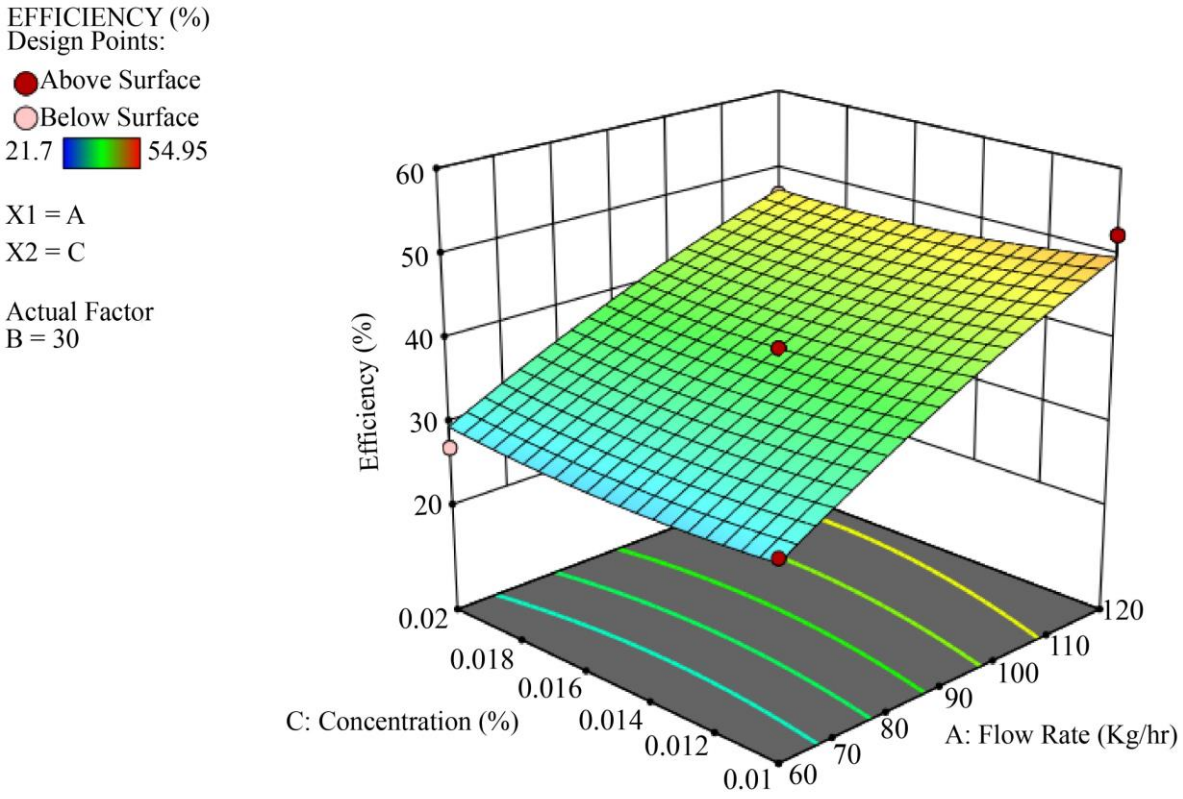

Fig. 14 Efficiency with respect to concentration and flow rate

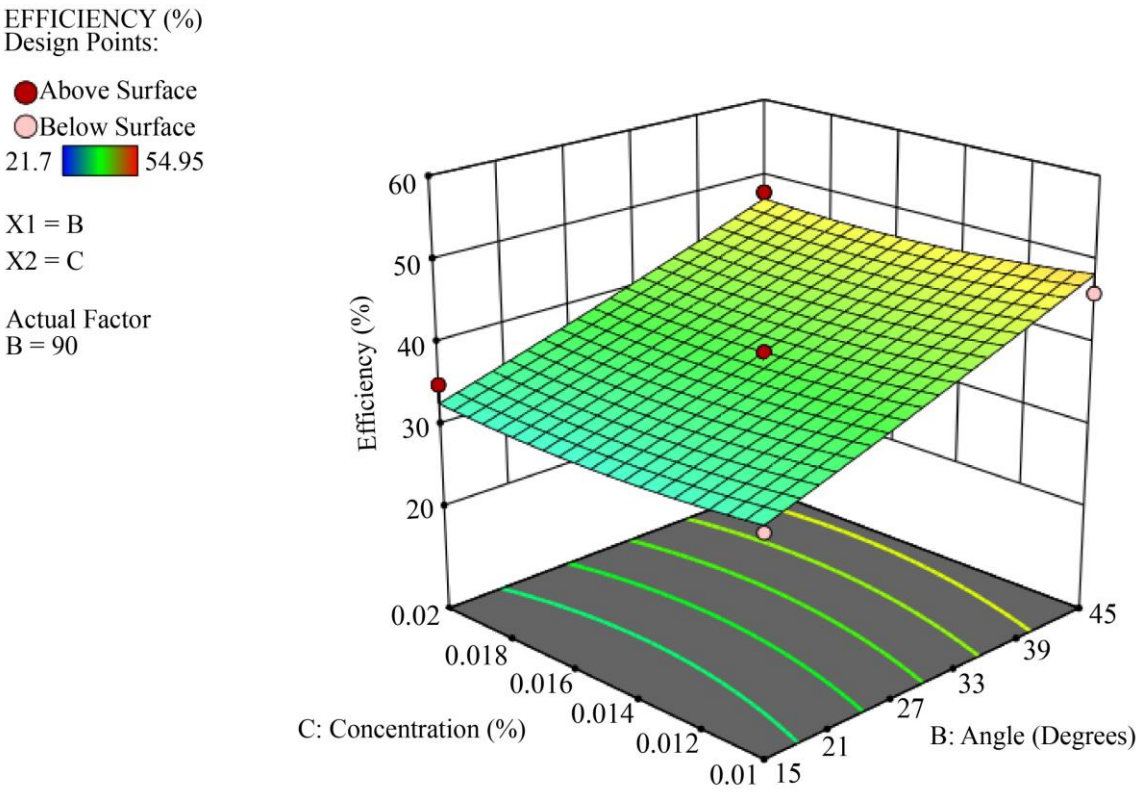

Fig. 15 Efficiency with respect to concentration and angle

As the slope angle grows linearly, the efficiency progressively rises. Although the interaction effect has the same impact, its efficiency value is greater than that of the inclination angle's linear effect. Efficiency is increased at both higher and lower ranges of flow rate by the linear influence of the angle of slope. The highest efficiency is achieved at greater flow rates with the angle of slope, as shown in Figure 13. The reciprocity impact extends beyond the linear impact of concentration and flow rate, as illustrated in Figure 14.

The area between greater values of both components is where the highest efficiency of 54.95% is found. Although it is relatively less effective than the interaction effect, the linear effect of concentration raises efficiency as the flow rate increases. The interaction impact outweighs the linear impacts of the angle of slope and concentration, as shown in Figure 15. The reciprocity impacts are more effective than the linear ones, even though efficiency has increased. Combined, a region with higher values is more efficient quickly because of carbon atoms in Bees wax Phase change materials and good thermal conductivity of Fe_3O_4.

7.2. Effect of Heat Gained by the Operating Fluid on Various Input Parameters of NEBPCM (Bees Wax + Fe_3O_4) and 2% Hybrid Nanocoating with Working Fluid as Water

Table 7 displays the findings of the ANOVA that was performed on the data collected for the experiment. The gotten F-value of 16.11 implies the model is substantial. There is only a 0.07% chance that an F-value this large could occur due to noise. Model terms are considered important if "Prob > F" is less than 0.0500. The model's goodness of fit can be explained by the R2, so in that instance, it is 0.9539. This suggests that less than 5% of the variants are not explained by the model and that ninety-five percentage of the results from the experiment were consistent with the data anticipated adjacent to the approach. When compared to the predicted R2 (0.2632), the modified R2 value (0.8947) is reasonable. Adequate accuracy is used to measure the signal-to-noise proportion. It turns out to be 14.6196, a definite sign that the model is sufficient. Equation (3) is the final equation produced by DOE.

Table 7. ANOVA table for heat gained by the operating fluid (Response 2)

Response 2 **Heat gained by the operating fluid Qc** **ANOVA for Response Surface Quadratic Model** **Analysis of variance table [Partial sum of squares – Type III]**						
Source	**Sum of Squares**	**df**	**Mean Square**	**F-value**	**p-value**	
Model	4.63	9	0.5143	16.11	0.0007	significant
A-FLOW RATE	4.31	1	4.31	134.98	< 0.0001	
B-ANGLE	0.0724	1	0.0724	2.27	0.1757	
C-CONCENTRATION	0.0134	1	0.0134	0.4213	0.5370	
AB	0.0327	1	0.0327	1.03	0.3450	
AC	0.0120	1	0.0120	0.3756	0.5593	
BC	0.0030	1	0.0030	0.0930	0.7692	
A^2	0.0384	1	0.0384	1.20	0.3091	
B^2	0.1188	1	0.1188	3.72	0.0950	
C^2	0.0313	1	0.0313	0.9808	0.3550	
Residual	0.2235	7	0.0319			
Lack of Fit	0.2235	3	0.0745			
Pure Error	0.0000	4	0.0000			
Cor Total **Std.Dev**	4.85 0.1787	16	R-Squared	0.9539		
Mean	2.96		Adjusted R^2	0.8947		
C.V. %	6.03		Predicted R^2	0.2632		
PRESS	3.58		Adeq Precision	14.6196		

Final equation in terms of coded factors: Heat gain by the cold fluid (Qc) = 3.044 + 0.733894 * A + 0.095144 * B + -0.041 * C + -0.090462 * AB + -0.05475 * AC + -0.02725 * BC + -0.095481 * A^2+ -0.167981 * B^2+ 0.086231 * C^2 (3)

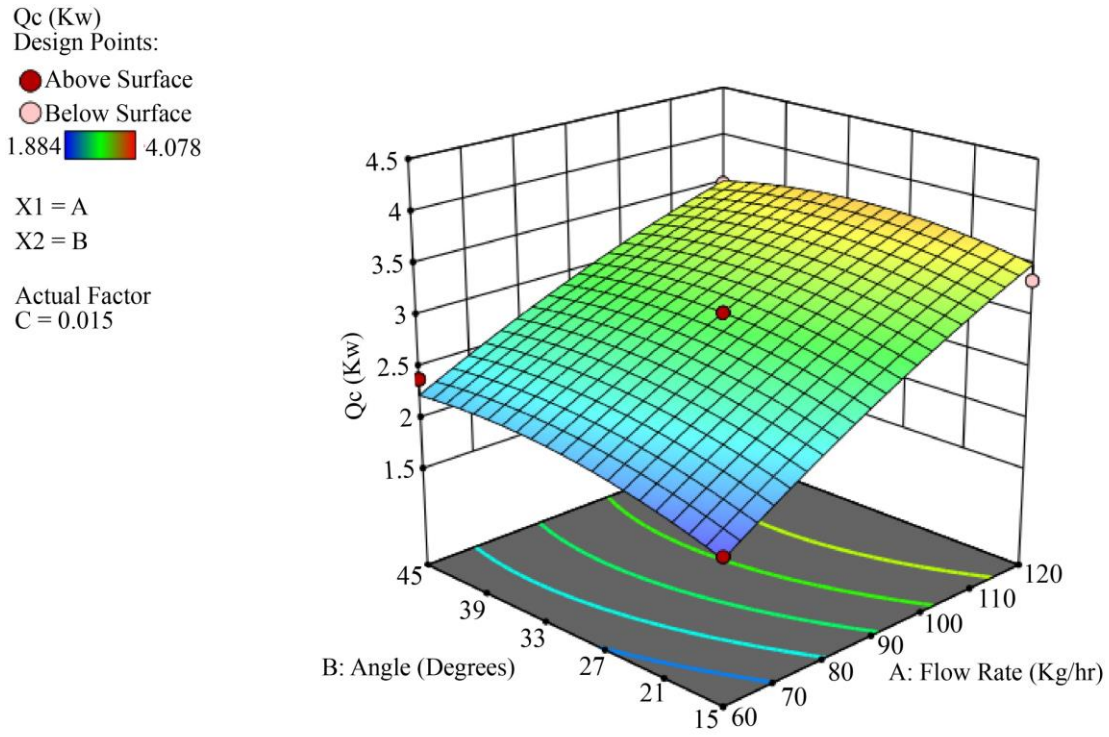

Fig. 16 Heat gained by the operating fluid (Qc) with respect to angle and flow rate

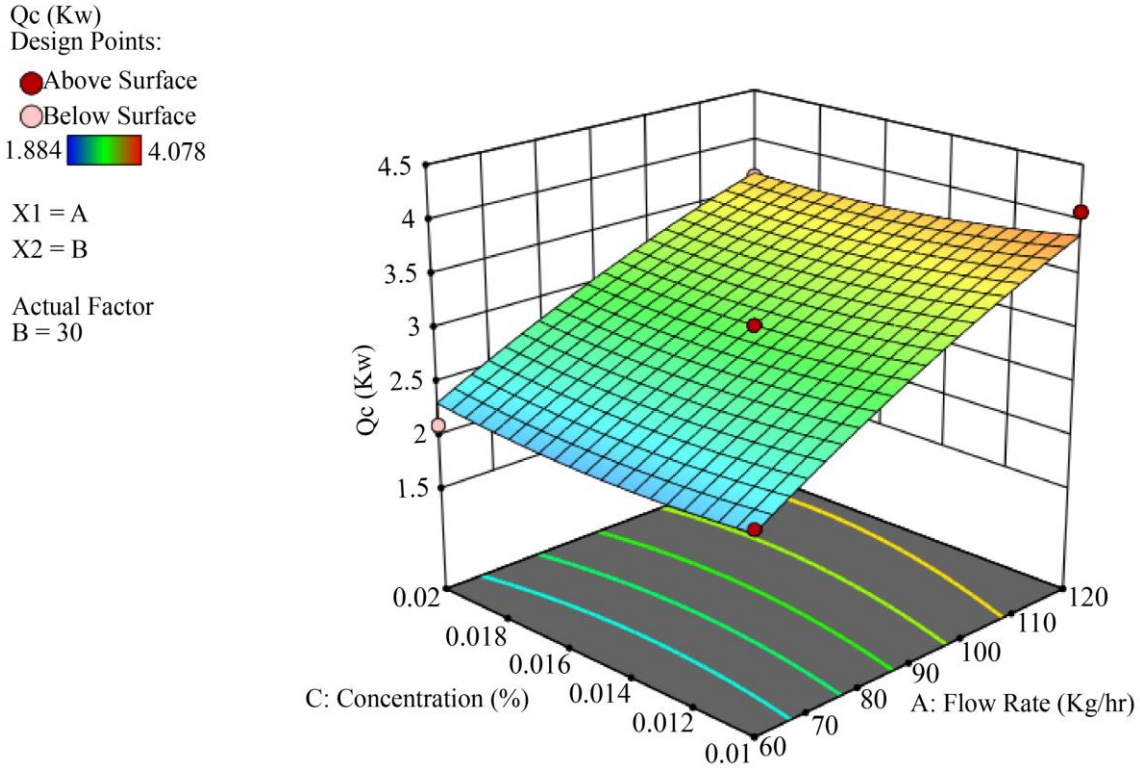

Fig. 17 Heat gained by the operating fluid (Qc) with respect to concentration and flow rate

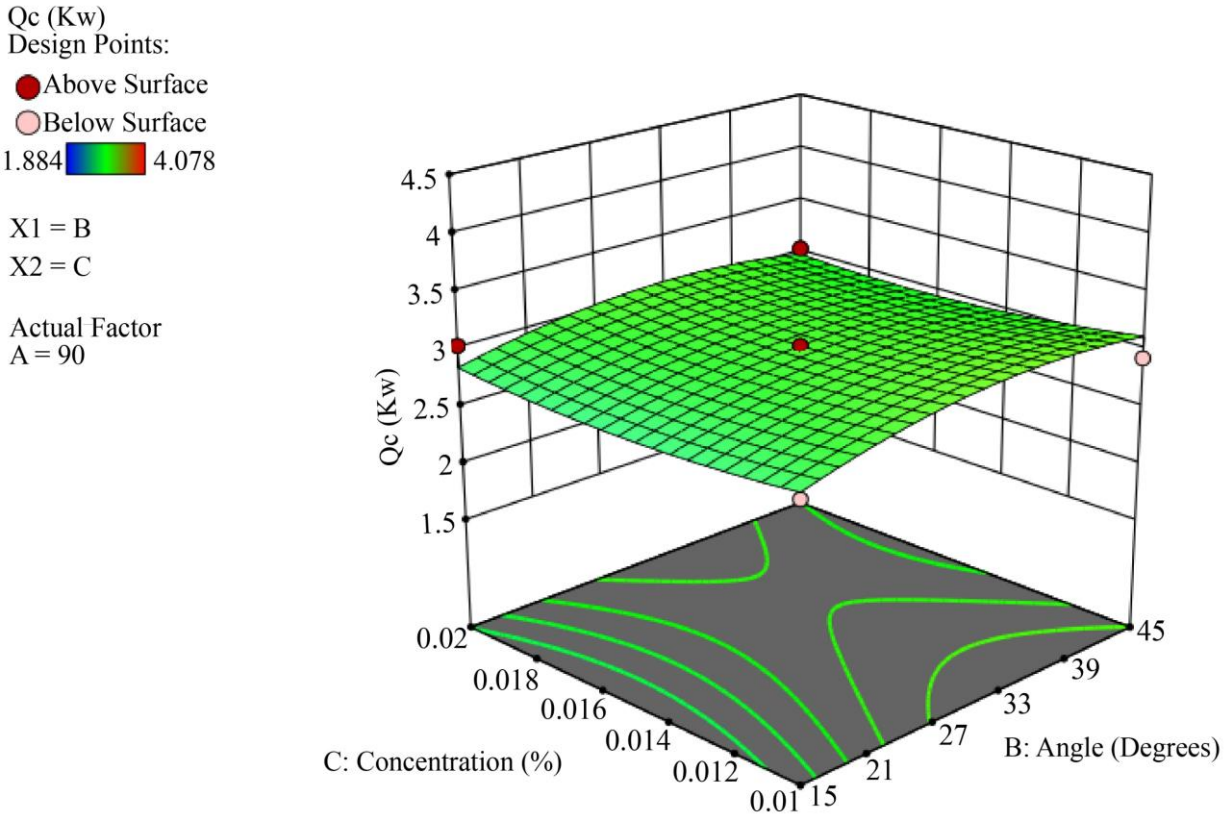

Fig. 18 Heat gained by the operating fluid (Qc) with respect to concentration and angle

Figure 16 shows the mesh diagram showing how the working fluid's (Qc) heat gain is affected by the rate of flow and tilt angle. The heat gained by the operating fluid or energy that can be used (Qc) gradually increases with the increase of flow rate. The working liquids (Qc) heat gain is marginally increased in the linear influence of the tilt angle. There is a slight improvement in the interaction impact on energy that can be used (Qc); the maximum energy that can be used (Qc) is reached in the middle of both factors. The fluid rate rises sharply, and the energy that can be used (Qc) when the flow velocity is greater. The maximum thermal gain is 3.49615 Kw by the operating fluid (Qc) achieved over a wide range of flow rates, as shown in Figure 17 grid chart. The interplay between the slope angle and the concentration of heat gained by the operating fluid (Qc) is shown in Figure 18. The effect of the degree of tilt on heat gained by the operating fluid (Qc) increases mid of the curve and, after that, slightly decreases. Where an increase in concentration increases the heat that the running fluid absorbs (Qc). When the concentration and the tilt angle have the impact of a combination, it is seen that this raises the heat gained by the operating fluid (Qc) sharply because copper tubes are employed in flat plate collectors for solar water heaters, the absorber plate receives direct sunlight, collectors surface area is large, and copper has a high thermal conductivity.

7.3. Comparison of All Parameters

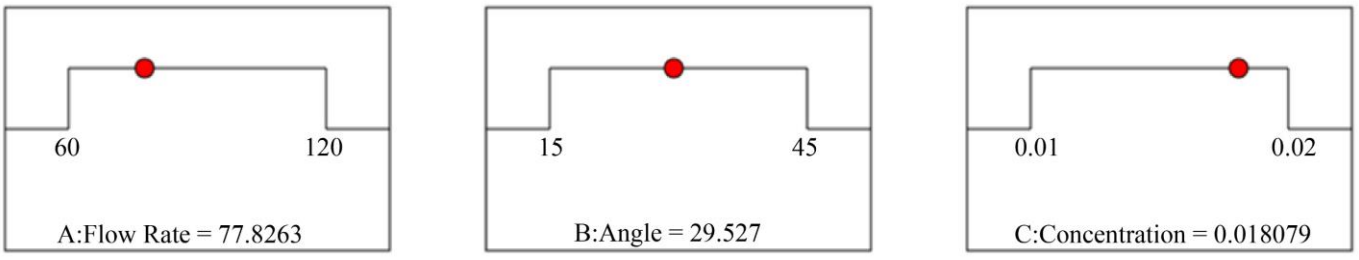

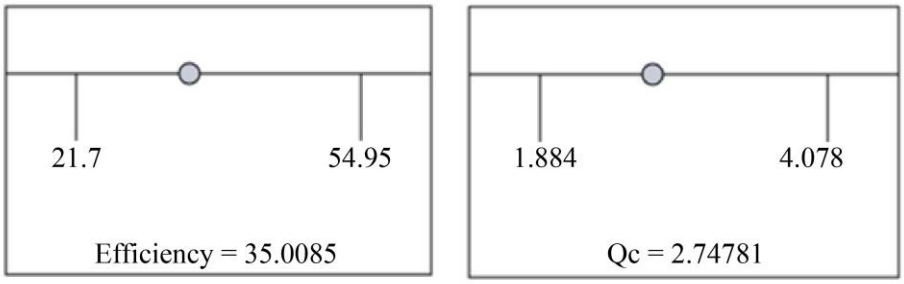

Fig. 19 Optimized parameters for solar flat plate collector using hybrid nanocoating and NEBPCM

7.4. Comparison Table

Table 8. Comparison of experimental results with optimized value

Parameters		RSM Value	Actual value
Optimized Operating parameters	Flow Rate	77.826	80
	Angle	29.527	30
	Concentration	0.018	0.02
Response	Efficiency	35.008	38.842
	% Deviation	3.834	
	Qc	2.748	2.964
	% Deviation	0.216	

A flow rate of 81.24, an angle of 35°, and a concentration of 0.02 are the parameters used in the system's testing or analysis. The Response Surface Methodology (RSM) predicts an efficiency of 35.008% under these ideal circumstances; however, the repeated experimental value is 38.842%. The difference between the experimental and RSM results is within a 5% margin of error. This satisfactory degree of accuracy validates the model.

8. Conclusion

A flat plate Solar Water Heating (SWH) system was designed, fabricated, and field-installed for performance evaluation in Chirala, the southern part of India (15.8167°N, 80.3587°E). The performance evaluation was conducted under actual solar conditions with three distinct test configurations, namely, with Baseline SWH with 0.01 wt% Fe_3O_4 nano-enhanced bio-based PCM, Intermediate concentration of 0.015 wt% Fe_3O_4-NEBPCM and High concentration of 0.02 wt% Fe_3O_4-NEBPCM, respectively. The Fe_3O_4 nano-embedded beeswax Phase Change Material (PCM) used in the hybrid-coated solar flat-plate water heater was tested over a 24-hour cycle from 6:00 am to 6:00 pm. This experiment was designed and analyzed using a Box-Behnken approach in the Design of Experiments (DOE) framework to evaluate the collector's performance. The performance was measured in two cases, focusing on two output parameters: 1) efficiency and 2) heat energy (Qc). The study examined the effects of three varying input parameters: Fe_3O_4 nanoparticle concentration in beeswax, Collector angle and water flow rate. The best results were achieved with a 0.015% Fe_3O_4 concentration in the beeswax PCM. This yielded an efficiency of 38.842% under optimal conditions derived from the DOE and Box-Behnken design. During the early morning, the system achieved a peak efficiency of 54.95% due to maximum heat absorption. The PCM, placed directly beneath the flat plate collector, functions as a thermal energy exchanger, transferring heat efficiently at night. The high carbon content of beeswax enhances heat transmission to the collector.

Additionally, the hybrid nanocoating on the collector broadens the absorption area, further boosting efficiency. In the morning, the PCM liquefies, and the hybrid-coated collector plate, with its increased absorptive surface, absorbs more solar radiation. This improved absorption boosts the efficiency to maximum levels, enhancing heat gain (Qc) similarly. This dual effect of thermal storage and enhanced absorption optimizes the system's performance throughout the day and night.

Nomenclature

BBD	- Box-Behnken Design
Al_2O3	- Aluminium III Oxide
RSM	- Response Surface Methodology
DOE	- Design of Experiments
FPC	- Flat Plate Collector
ID	- Inner Diameter
OD	- Outer Diameter
Fe_3O_4	- Iron II III Oxide
SWH	- Solar water heater
FTIR	- Fourier transform infrared spectroscopy
DSC	- Differential scanning calorimetry
PCM	- Phase Change Material
NEBPCM	- Nano Embedded Bees Wax Phase Change Material

References

[1] Ebru Kavak Akpinar, and Fatih Koçyiğit, "Energy and Exergy Analysis of a New Flat-Plate Solar Air Heater Having Different Obstacles on Absorber Plates," *Applied Energy*, vol. 87, no. 11, pp. 3438-3450, 2010. [CrossRef] [Google Scholar] [Publisher Link]

[2] World Health Organization, News Release, 2014. [Online]. Available: https://www.who.int/mediacentre/news/releases/2014/air-pollution/en/

[3] Soroush Ebadi et al., "Melting of Nano-PCM Inside a Cylindrical Thermal Energy Storage System: Numerical Study with Experimental Verification," *Energy Conversion and Management*, vol. 166, pp. 241-259, 2018. [CrossRef] [Google Scholar] [Publisher Link]

[4] Shivika Mittal et al., "Bridging Greenhouse Gas Emissions and Renewable Energy Deployment Target: Comparative Assessment of China and India," *Applied Energy*, vol. 166, pp. 301-313, 2016. [CrossRef] [Google Scholar] [Publisher Link]

[5] Jay Squalli, "Renewable Energy, Coal as a Base Load Power Source, and Green- House Gas Emissions: Evidence from US State-Level Data," *Energy*, vol. 127, pp. 479-488, 2017. [CrossRef] [Google Scholar] [Publisher Link]

[6] Claudia Furlan, and Cinzia Mortarino, "Forecasting the Impact of Renewable Energies in Competition with Non-Renewable Sources," *Renewable and Sustainable Energy Reviews*, vol. 81, no. 2, pp. 1879-1886, 2018. [CrossRef] [Google Scholar] [Publisher Link]

[7] "*International Energy Agency, Renewables*," Report, 2018. [Publisher Link]

[8] Ali H.A. Al-Waeli et al., "Comparison of Prediction Methods of PV/T Nanofluid and Nano-PCM System using a Measured Dataset and Artificial Neural Network," *Solar Energy*, vol. 162, pp. 378-396, 2018. [CrossRef] [Google Scholar] [Publisher Link]

[9] Xinyu Zhang et al., "Experimental Investigation of the Higher Coefficient of Thermal Performance for Water-in-Glass Evacuated Tube Solar Water Heaters in China," *Energy Conversion and Management*, vol. 78, pp. 386-392, 2014. [CrossRef] [Google Scholar] [Publisher Link]

[10] Zhijian Liu et al., "Design of High-Performance Water-In-Glass Evacuated Tube Solar Water Heaters by a High-Throughput Screening based on Machine Learning: A Combined Modeling and Experimental Study," *Solar Energy*, vol. 142, pp. 61-67, 2017. [CrossRef] [Google Scholar] [Publisher Link]

[11] P. Manoj Kumar, and K. Mylsamy, "Experimental Investigation of Solar Water Heater Integrated with a Nanocomposite Phase Change Material," *Journal of Thermal Analysis and Calorimetry*, vol. 136, pp. 121-132, 2018. [CrossRef] [Google Scholar] [Publisher Link]

[12] Alexios Papadimitratos et al., "Evacuated Tube Solar Collectors Integrated with Phase Change Materials," *Solar Energy*, vol. 129 pp. 10-19, 2016. [CrossRef] [Google Scholar] [Publisher Link]

[13] Mohammad Ali Fazilati, and Ali Akbar Alemrajabi, "Phase Change Material for Enhancing Solar Water Heater, an Experimental Approach," *Energy Conversion and Management*, vol. 71, pp. 138-145, 2013. [CrossRef] [Google Scholar] [Publisher Link]

[14] P. Manoj Kumar et al., "Study on Thermal Conductivity of the Candle Making Wax (CMW) using Nano-TiO_2 Particles for Thermal Energy Storage Applications," *AIP Conference Proceedings: International Conference on Materials, Manufacturing and Machining*, Tamilnadu, India, vol. 2128, no. 1, 2019. [CrossRef] [Google Scholar] [Publisher Link]

[15] Mohammed Mumtaz A. Khan et al., "Evaluation of Solar Collector Designs with Integrated Latent Heat Thermal Energy Storage: A Review," *Solar Energy*, vol. 166, pp. 334-350, 2018. [CrossRef] [Google Scholar] [Publisher Link]

[16] Mohamed E. Zayed et al., "Applications of Cascaded Phase Change Materials in Solar Water Collector Storage Tanks: A Review," *Solar Energy Materials and Solar Cells*, vol. 199, pp. 24-49, 2019. [CrossRef] [Google Scholar] [Publisher Link]

[17] H. Sheng Xue, "Experimental Investigation of a Domestic Solar Water Heater with Solar Collector Coupled Phase-Change Energy Storage," *Renewable Energy*, vol. 86, pp. 257-261, 2016. [CrossRef] [Google Scholar] [Publisher Link]

[18] Wei Wu et al., "Experimental Study on the Performance of a Novel Solar Water Heating System with and Without PCM," *Solar Energy*, vol. 171, pp. 604-612, 2018. [CrossRef] [Google Scholar] [Publisher Link]

[19] Mohamed Hany Abokersh et al., "Review of the Phase Change Material (PCM) usage for Solar Domestic Water Heating Systems (SDWHS)," *International Journal of Energy Research*, vol. 42, pp. 329-357, 2018. [CrossRef] [Google Scholar] [Publisher Link]

[20] Shin Yiing Kee, Yamuna Munusamy, and Kok Seng Ong, "Review of Solar Water Heaters Incorporating Solid-Liquid Organic Phase Change Materials as Thermal Storage," *Applied Thermal Engineering*, vol. 131, pp. 455-471, 2018. [CrossRef] [Google Scholar] [Publisher Link]

[21] P. Manoj Kumar et al., "Experimental Investigations on Thermal Management and Performance Improvement of Solar PV Panel using a Phase Change Material," *AIP Conference Proceedings: International Conference on Materials, Manufacturing and Machining*, Tamilnadu, India, vol. 2128, no. 1, 2019. [CrossRef] [Google Scholar] [Publisher Link]

[22] George V. Belessiotis et al., "Preparation and Investigation of Distinct and Shape Stable Paraffin/SiO_2 Composite PCM Nanospheres," *Energy Conversion and Management*, vol. 168, pp. 382-394, 2018. [CrossRef] [Google Scholar] [Publisher Link]

[23] P. Manoj Kumar, K. Mylsamy, and P.T. Saravanakumar, "Experimental Investigations on Thermal Properties of Nano-SiO_2/Paraffin Phase Change Material (PCM) for Solar Thermal Energy Storage Applications," *Energy Sources, Part A: Recovery, Utilization, and Environmental Effects*, vol. 42, no. 19, pp. 2420-2433, 2020. [CrossRef] [Google Scholar] [Publisher Link]

[24] Zakir Khan, Zulfiqar Khan, and Kamran Tabeshf, "Parametric Investigations to Enhance Thermal Performance of Paraffin Through a Novel Geometrical Configuration of Shell and Tube Latent Thermal Storage System," *Energy Conversion and Management*, vol. 127, pp. 355-365, 2016. [CrossRef] [Google Scholar] [Publisher Link]

[25] Jialin Yang et al., "Experimental Study on Enhancement of Thermal Energy Storage with Phase-Change Material," *Applied Energy*, vol. 169, pp. 164-176, 2016. [CrossRef] [Google Scholar] [Publisher Link]

[26] P. Manoj Kumar et al., "Investigating Thermal Properties of Nanoparticle Dispersed Paraffin (NDP) as Phase Change Material for Thermal Energy Storage," *Materials Today: Proceedings*, vol. 45, no. 2, pp. 745-750, 2021. [CrossRef] [Google Scholar] [Publisher Link]

[27] Lin Qiu et al., "Review on Micro/Nano Phase Change Materials for Solar Thermal Applications," *Renewable Energy*, vol. 140, pp. 513-538, 2019. [CrossRef] [Google Scholar] [Publisher Link]

[28] Hassan Nazir et al., "Recent Developments in Phase Change Materials for Energy Storage Applications: A Review," *International Journal of Heat and Mass Transfer*, vol. 129, pp. 491-523, 2019. [CrossRef] [Google Scholar] [Publisher Link]

[29] P. Manoj Kumar et al., "Experimental Investigation on Thermal Conductivity of Nanoparticle Dispersed Paraffin (NDP)," *Materials Today: Proceedings*, vol. 45, no. 2, pp. 735-739, 2021. [CrossRef] [Google Scholar] [Publisher Link]

[30] Farid Bahiraei, Amir Fartaj, and Gholam-Abbas Nazri, "Experimental and Numerical Investigation on the Performance of Carbon-Based Nano Enhanced Phase Change Materials for Thermal Management Applications," *Energy Conversion and Management*, vol. 153, pp. 115-128, 2017. [CrossRef] [Google Scholar] [Publisher Link]

[31] Swaroop Kumar Mandal et al., "Performance Investigation of CuO-Paraffin Wax Nanocomposite in Solar Water Heater during Night," *Thermochimica Acta*, vol. 671, pp. 36-42, 2019. [CrossRef] [Google Scholar] [Publisher Link]

[32] Y.Q. Li et al., "Numerical Analysis and Parameters Optimization of Shell and-Tube Heat Storage Unit Using Three Phase Change Materials," *Renewable Energy*, vol. 59, pp. 92-99, 2013. [CrossRef] [Google Scholar] [Publisher Link]

[33] Gianluca Serale et al., "Characterization and Energy Performance of a Slurry PCM-based Solar Thermal Collector: A Numerical Analysis," *Energy Procedia*, vol. 48, pp. 223-232, 2014. [CrossRef] [Google Scholar] [Publisher Link]

[34] Lei Yang, Xiaosong Zhang, and Guoying Xu, "Thermal Performance of a Solar Storage Packed Bed using Spherical Capsules Filled with PCM Having Different Melting Points," *Energy and Buildings*, vol. 68, pp. 639-646, 2014. [CrossRef] [Google Scholar] [Publisher Link]

[35] Nandy Putra, Erwin Prawiro, and Muhammad Amin, "Thermal Properties of Beeswax/Cuo Nano Phase-Change Material Used for Thermal Energy Storage," *International Journal of Technology*, vol. 7, no. 2, pp. 244-253, 2016. [CrossRef] [Google Scholar] [Publisher Link]